RSC Advances

PAPER

Check for updates

Cite this: *RSC Adv.*, 2022, **12**, 17853

Adsorption of CO over the Heusler alloy CrCoIrGa(001) surface: first-principles insights

Abdelazim M. Mebed,[ab] Muhammad Mushtaq, *[c] Muhammad Faizan, [d] Riadh Neffati,[e] Amel Laref,[f] Sumegha Godara[g] and Sana Maqbool[h]

In this study, the adsorption of CO molecule over (001) surface of the Heusler alloy CrCoIrGa, has been investigated using DFT+U calculations. It is demonstrated that, after relaxation, the (001) surface retains the bulk atomic positions, exhibiting no apparent surface reconstruction. Owing to the emergence of unsaturated bonds at the surface, the surface layer atoms are found to carry more spin-polarization (SP) and atomic moments than that of inner layer atoms. The ground state total SP (magnetic moment) is found to be 27% (42.256 μ_B). To explore the CO adsorption over the surface, five different adsorption configurations (sites) are considered and the strength of CO to surface interaction is estimated from the computed density of states (DOS), adsorption energy (E_a), change in magnetic moment (ΔM), vertical height between molecule and surface (h), charge transfer (ΔQ), and charge density difference (CDD) plots. For all configurations, the E_a lies in the range of −2.15 to −2.34 eV, with CO molecule adsorbed on the top of Ir atom as the most favorable adsorption configuration. The observed E_a, ΔQ, h, and ΔM values, collectively predict that the (001) surface has strong interaction (chemisorption) with CO gas molecule, thus, might be useful in gas sensing applications.

Received 14th May 2022
Accepted 9th June 2022

DOI: 10.1039/d2ra03043h

rsc.li/rsc-advances

1. Introduction

The emission of toxic gases from motor vehicles and industries, significantly affects the environmental system by causing air pollution, climate changes and risks to human health. These gases can be categorized into organic pollutants such as benzene and ethanol, whereas inorganic ones include carbon monoxide (CO), ammonia (NH_3) and carbon dioxide (CO_2).[1] Unlike other gases, CO, the silent killer, does not exist in nature and is mainly produced through incomplete combustion of coal and fuels. In addition, combustion at low oxygen levels and low temperatures is known to produce CO. Being a colorless, tasteless, non-irritating and odorless gas, it is difficult to identify its effects and it cannot be detected without sensors and is thus far more dangerous to humans than other gases such as CO_2 and NH_3. Moreover, when inhaled, it reacts with oxygen carrying blood cells and blocks body organs from getting the oxygen they need, ultimately resulting in death. Thus, from an environmental and health point of view, it is of prime importance to design methods and devices which can detect and sense the CO gas and help in controlling its emission from the coil/fuel burning appliances.

Catalytic processes occur in nature and are used in industry as well as are extensively focused in scientific research for gas sensing purpose. The process of gas molecules adsorption over the solid surfaces is known as heterogeneous catalysis. Solids are widely used as catalysts because most of the chemical reactions take place at their surface and interface. The rate of chemical reactions taking place at a solid surface is found strongly dependent on the surface geometry and morphology. CO is one of the molecules most extensively studied in experiments and theories.[2–5] Vanadium–tin oxide based CO gas sensor was developed experimentally and it was found that vanadium redox pairs and oxygen vacancies play a key role in sensing mechanism.[6] In another study, copper (Cu) single atom anchored $Ti_3C_2T_x$ MXene sheets were demonstrated as effective and robust catalysts for electrochemical CO reduction and ultrahigh selectivity of 98% for the formation of multi-carbon products.[7] The adsorption of CO over Rh/CeO_2 studied experimentally with infrared (IR) spectroscopy in the temperate range of 90 to 300 K, reports that at 90 K, the observed IR peak at 2163 cm^{-1} is more sensitive to CO pressure than that noticed at 2186 cm^{-1}[8] The adsorption and dissociation of CO over Co–

[a]*Department of Physics, College of Science, Jouf University, Al-Jouf, Sakaka P. O. Box 2014, Saudi Arabia*

[b]*Physics Department, Faculty of Science, Assuit University, Assuit 71516, Egypt*

[c]*Department of Physics, University of Poonch Rawalakot, 12350, Pakistan. E-mail: mushtaq325@gmail.com*

[d]*Department of Physics, University of Peshawar, Peshawar, 25120, Pakistan*

[e]*Department of Physics, King Khalid University, P. Box 9032, Abha 61413, Kingdom of Saudi Arabia*

[f]*Department of Physics and Astronomy, College of Science, King Saud University, Riyadh, Saudi Arabia*

[g]*Louisiana Tech University, Louisiana, USA*

[h]*Department of Physics, Fatima Jinnah Women University, Rawalpindi, 46000, Pakistan*

This article is licensed under a Creative Commons Attribution-NonCommercial 3.0 Unported Licence.

(cc) BY-NC

Si(111) surface was examined using X-ray photo-electron spectroscopy (XPS), showing that room temperature CO adsorption takes place only at Co-rich condition.[9] Zhang *et al.* theoretically investigated the reactivity of the $Cu_3Pt(111)$, Pt(111) and Cu(111) surfaces towards CO and found that the molecule prefers to adsorb on an atop site of Pt.[10] It is found that multilayered porous graphene sheets strongly interact with CO, resulting in chemisorption with significant amount of charge exchange.[11] Despite tremendous achievements in the gas sensing field, it is of prime importance to comprehensively explore the adsorption mechanisms of CO over solid surfaces and the design of highly sensitive CO based gas sensors.

In recent years, owing to diverse structural, electronic, magnetic and thermoelectric properties, Heusler alloys have been a subject of active research.[12–17] These materials, have a great potential for spintronic devices, as evidenced by their high Curie temperature, and complete spin-polarization.[18–29] In particular, the experimental realization of Heuslers thin films makes them more attractive for practical applications.[30] The structure, electronic and magnetic properties of NbFeCrAl(001) and NbFeVGa(001),[31] CoNbMnSi(001),[32] TiZrCoAl(001) and TiZrCoAl(110),[33] CoMnZnSi(111)[34] have been reported in the literature. So far, the Heusler surfaces are mainly investigated for spin properties, and their capability for sensing toxic gas molecules has been ignored, except the very few reports.[35–37] Thus, the catalytic properties of such materials are less known. Far as we are aware, no study has been conducted on the CO adsorption over quaternary Heusler thin film surfaces. Driven by the potential scope of the metallic surfaces (*e.g.* Ni, Pt ones) in the adsorption and conversion of toxic gases,[38] herein, we explore the possibility of CrCoIrGa to be used for the adsorption of CO gas molecule. This study could initiate further research on the gas sensing capability of the Heuslers based surfaces. The manuscript is organized into following sections; (1) the structure, electronic and magnetic properties of the bulk and bare surfaces are explored, (2) gas sensing properties are examined by placing CO gas molecule over the various sites of the surface, (3) most favorable adsorption site is marked by comparing the adsorption energy of the considered sites, (4) the interaction between gas molecule and surface is estimated with adsorption energy, charge transfer, bond lengths, and electronic density of states.

2. Computational method

Density functional theory (DFT), integrated in the Vienna *Ab initio* Simulation Package (VASP) is widely used to predict the ground-state properties and adsorption of molecules on surfaces. The method involves expanding atomic orbitals in plane-wave basis set using pseudopotentials to solve the Kohn–Sham equations and estimate the total energy.[39] The exchange-correlation potential is presented using the generalized gradient approximation (GGA) of Perdew–Burke–Ernzerhof (PBE) formalism.[40] Initially the unit cell (u.c) structure of bulk CrCoIrGa (in POSCAR format) is fully relaxed for atomic positions and lattice vectors. The adsorption properties of CO gas molecule are examined over the CoIr-terminated CrCoIrGa(001) surface having; seven atomic layers, in-pane (*xy*) surface area of (8.39×8.39) Å^2, vertical thickness of 23.9 Å (along *z*-axis) and a vacuum space of 15 Å along *z*-direction to ensure the insulation and isolation between the surface and its periodic images. The bottom four layers are kept fixed to bulk positions, while the top three layers of the system (without and with CO) are fully relaxed by giving freedom to both motions of the lattice vectors and the atomic positions until the convergence of total energy with tolerance of less than 10^{-4} eV. The Brillouin-zone sampling is performed using the known Monkhorst–Pack algorithm [MP]. A *K*-points grid of $8 \times 8 \times 1$ is used for charge density and more refined grid of $12 \times 12 \times 1$ is used for the density of states (DOS) calculations. An energy cut-off of 500 eV is employed for the expansion of plane wave basis set. Besides, the long-range van der Waal like interactions are described within the scheme of the dispersion of Grimme (*i.e.* DFT-D3).[41] It is well understood that normal DFT fails to accurately predict the electronic properties of d-block elements and their compounds, and desperately need a correction term to be included for the proper estimation of electronic interactions. For this purpose, to perform DFT+U calculations, Hubbard parameter *U* (of 3 eV) has been added for correlated d-orbitals.[42,43] The reliability of the computational parameters is verified by calculating the geometry (bond length/angle), and electronic properties (density of states) of the isolated CO molecule, and compared with literature.

In order to investigate the CO adsorption on the CrCoIrGa(001) surface, a slab model is considered by building a $2 \times 2 \times 1$ supercell with a sufficient vacuum along the c-vector. Depending on the surface geometry, molecule is adsorbed over five different adsorption sites and adsorption energy E_a is calculated using eqn (1), as given below

$$E_a = E_{surf\text{-}CO} - E_{surf} - E_{CO} \quad (1)$$

where $E_{surf\text{-}CO}$, E_{surf} and E_{CO} stand for the total energy of CO+surface system, bare surface (*i.e.* without CO), and isolated CO molecule, respectively.

3. Results and discussion

3.1. Bulk and bare (001) surface

Structural properties. The quaternary Heusler alloys (QHAs) are known to be composed of four distinct elements with composition ratio 1 : 1 : 1 : 1, XX′YZ formula, and can be found in three phases, Y1, Y2 and Y3, where each phase belongs to the same crystal system (face-centered cubic, space group $Fd\bar{4}3m$ #216).[44] These phases are obtained by interchanging the Wyckoff positions among X, X′, Y and Z atoms. Our results show that the given alloy is intrinsically ferromagnetic (FM) with optimized lattice constant of 5.93 Å, and has Y3 as the most stable phase, being consistent with our previous study.[45]

The fully relaxed surface structure is shown in Fig. 1(a–d). It can be seen that, geometry of the surface is kept well after relaxation. The surface model is composed of seven atomic layers; three of them are formed by Cr and Ga atoms (CrGa-layers), and rest of four layers are constituted by Co and Ir

© 2022 The Author(s). Published by the Royal Society of Chemistry

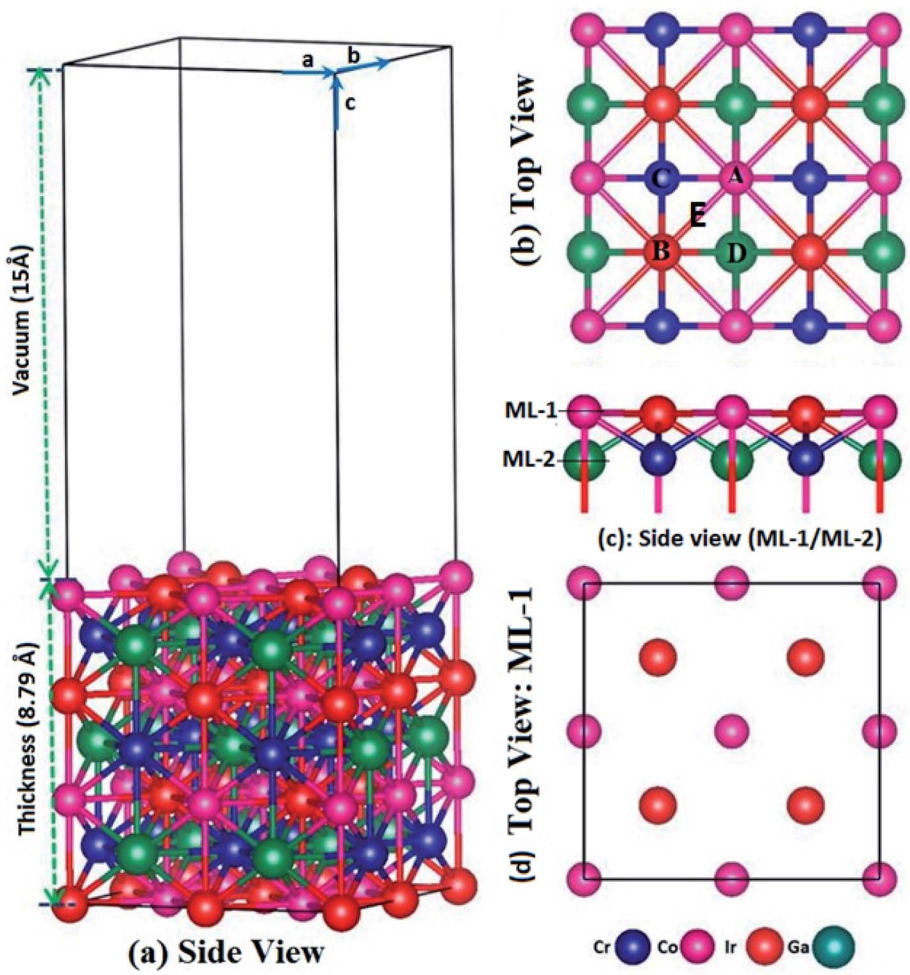

Fig. 1 Relaxed geometry of CrCoIrGa(001) surface; (a) side view, (b) top view, (c) side view of the first/second atomic layer (ML-1)/(ML-1), (d) top view of the ML-1. The selected adsorption sites are marked by letter A, B, C, D and E in panel (b). The structures are visualized with VESTA software.[47]

atoms (CoIr-layers). These layers repeat alternatively along the **c**-vector such that the first (the top most layer, designated as ML-1), third, fifth and seventh layer contains Co and Ir atoms, while the second (ML-2), fourth and sixth layer has only Cr and Ga atoms. The calculated vertical distance between ML-1 and ML-2 is found to be 1.32 Å, being shorter than the actual value of 1.43 Å. The reason is that, ML-1 atoms being coordinated with a few atoms in comparison with inner layer atoms, move downward after relaxation to get stabilized. In addition, the observed inter atomic distance d_{Cr-Ga} is 2.44 Å being decreased from the initial value of 2.56 Å. Similarly, the d_{Co-Ir} also reduces to 2.51 Å from the actual value of 2.56 Å. The final (initial) inta-plane Cr–Cr, Ga–Ga, Ir–Ir, and Co–Co distances, all are found to be 4.19 Å (4.19 Å). Meanwhile, within ML-1 (ML-2), the Co–Ir (Cr–Ga) bond length is 2.967 Å, negligibly changed (0.2%) from the value of 2.966 Å. The inta-plane Ir–Co–Ir (Cr–Ga–Cr) bond angles also undergo minor deviation (decreased from 90° to 89.97°). These findings show that geometry of the present surface is kept well after relaxation, except minor deviations in the top most layers.

Electronic and magnetic properties. Cutting the bulk material into two-dimensional (2D) like thin film surfaces, might bring interesting changes in the electronic and magnetic properties. To explore how these properties evolve from the surface, the total, partial and orbital electronic density of states are computed shown in Fig. 2(a–k), whereas, the magnetic properties are quantitatively explored with magnetic moment data shown in Table 1. From the total DOS (hereafter TDOS) in Fig. 2(a), it is found that both majority and minority electronic states cross the Fermi level (E_F), confirming the metallic behavior of the surface. The electronic states lie in the energy range −15 to −14 eV and from −10 to 10 eV. The emergence of energy states in these regions can be well understood from the partial DOS (PDOS) and orbital DOS (ODOS) plots, provided in Fig. 2(b–k). It is noticed that electronic states emerging around −14 eV, mainly belong to Ga atoms, whereas the states just below and above the E_F come from Cr, Co and Ir atoms. The ODOS of transition metal atoms Cr, Co and Ir reveals that d-orbitals of these elements have an important role in the formation of energy states across the E_F and result in metallic

© 2022 The Author(s). Published by the Royal Society of Chemistry

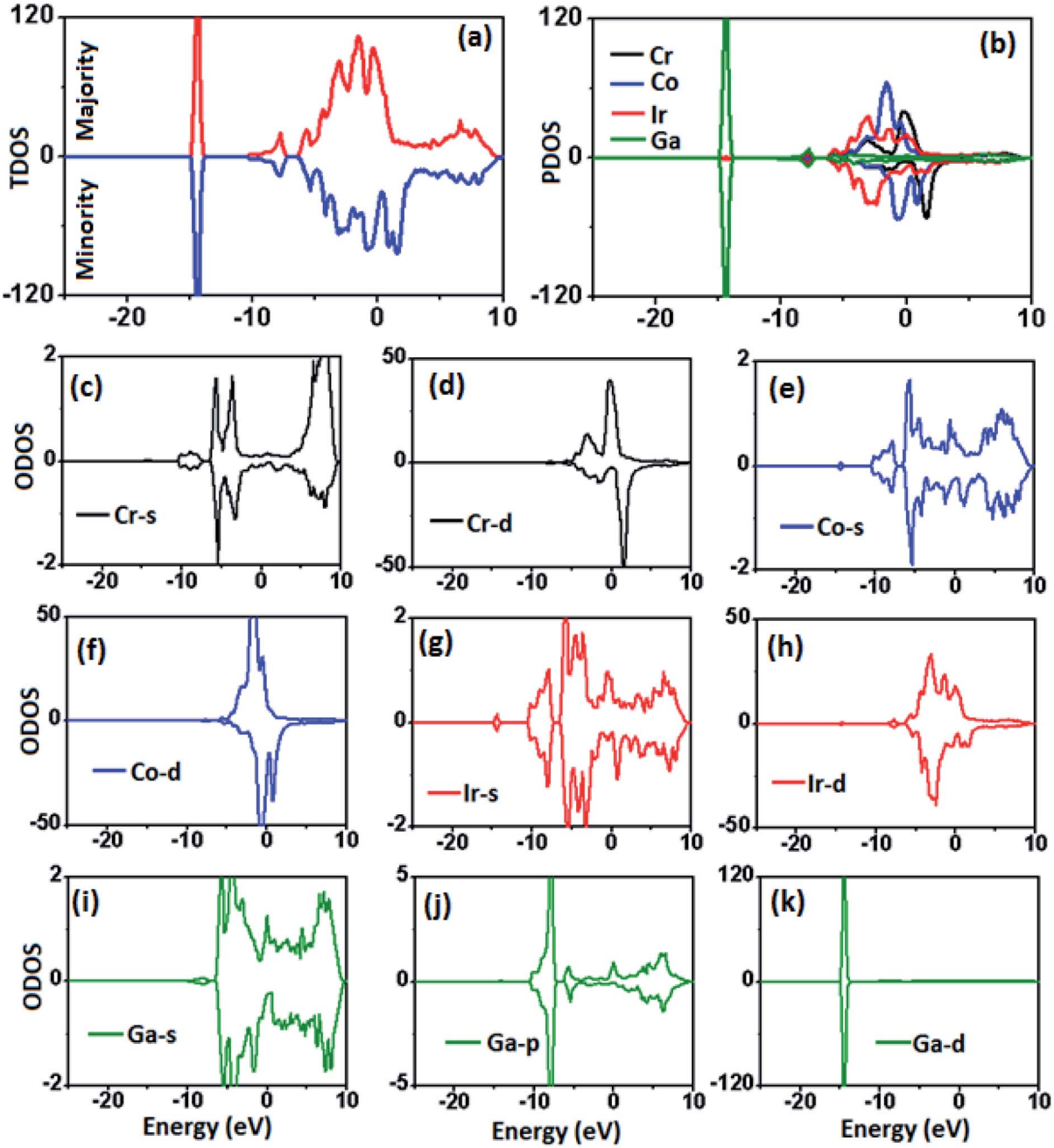

Fig. 2 (a) TDOS for pristine surface, (b) PDOS for constituent atoms, (c–e) ODOS for Cr-atoms, (f–h) ODOS for Co-atoms, (i–k) ODOS for Ga-atoms.

Table 1 Adsorption energy E_a (eV), charge transfer between molecule and surface $\Delta Q|e|$ (negative value means substrate donates charge to molecule), optimized vertical distance between molecule and surface h (Å), surface to molecule nearest atom to atom distance d (Å), C–O bond length d_{C-O}, Fermi energy E_F (eV), total magnetic moment M_p (μ_B) of the pristine surface, total magnetic moment of the CO adsorbed surface M_a (μ_B), change in total magnetic moment $\Delta M=(M_a - M_a)$ and spin-polarization SP (%) calculated at DFTD3 level for various adsorption configurations. The negative value of ΔQ demonstrates transfer of charge from surface to gas molecule[a]

System	E_a	ΔQ	h	d_{min}	d_{C-O}	E_F	M_p	M_a	ΔM	SP
A-site	−2.155	−0.278	1.634	1.74	1.17	1.4549	42.256	41.808	−0.448	23
B-site	−2.344	−0.218	1.863	1.875	1.16	1.4789	42.256	42.795	0.539	16
C-site	−2.310	−0.207	1.887	1.871	1.17	1.4777	42.256	43.223	0.967	26
D-site	−2.250	−0.242	1.743	1.735	1.16	1.4594	42.256	42.768	0.512	20
E-site	−2.208	−0.331	1.481	1.80	1.18	1.4325	42.256	42.768	0.512	29

[a] Pristine CrCoIrGa(001) surface: $E_F = 1.462$ eV, SP = 27%.

© 2022 The Author(s). Published by the Royal Society of Chemistry

property of the surface. Moreover, the sharp symmetric peak around −14 eV below the E_F is attributed to Ga-p/d orbital. The presence of atomic p/d orbitals of the constituent atoms in the energy range −8 eV to E_F evidences strong hybridization between them. For all constituent atoms, in comparison with p/d orbitals, the s-orbitals have very small contribution in DOS, indicating less significant role in the electronic properties of the surface.

Magnetic properties of the surfaces play a vital role in chemical reactivity, and information processing, *etc.* To explore these properties, atomic and total magnetic moments are computed, and their origin can be extracted from the ODOS plots. The Co atoms in middle layers have moment of 1.19 μ_B, which increases to 1.69 μ_B in ML-1. For Cr atoms, the inner layer moment is 1.19 μ_B, and becomes 1.37 μ_B in ML-2. The Ir and Ga atoms carry very small moments of less than 0.2 μ_B. For example, in lower layers, Ir moment is 0.11 μ_B, which changes to −0.02 μ_B in outer layers. The moment of Ga atom is found to be −0.03 μ_B. In Fig. 2(e and f), one can observe that Co-s orbital is well symmetric in two spin channels, but Co-d orbital has asymmetric shape around E_F, demonstrating that magnetic moment of Co atoms is mainly caused by the splitting of d-orbitals. Similarly, the moment of Cr and Ir atoms is also contributed by the asymmetric distribution of d-orbitals. The negative moment of Ga atoms predicts opposite spin-

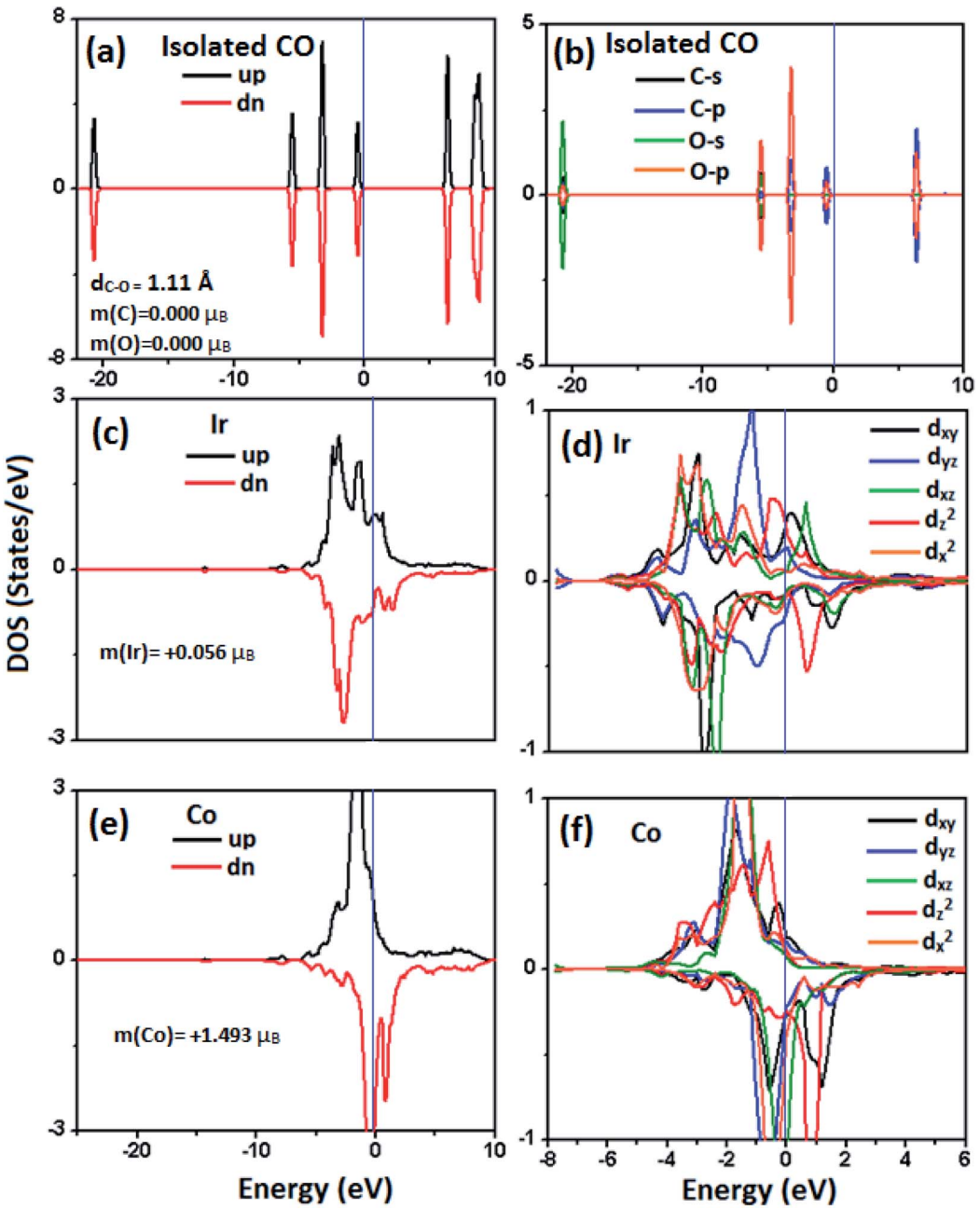

Fig. 3 (a, b) TDOS and PDOS for isolated CO molecule, (c, d) PDOS and ODOS for Ir-atoms, (e, f) PDOS and ODOS for Co-atoms.

© 2022 The Author(s). Published by the Royal Society of Chemistry

polarization of these atoms caused by the exchange to charge transfer with neighboring atom.

3.2. Adsorption of CO over CrCoIrGa(001) surface

As discussed above, the chemical property of a surface is strongly controlled by the atoms present in the top layer of the surface. These atoms are assumed to have un-paired electrons, available for chemical bonding with external species/molecules. For a surface containing two or more than two different elements, there might be multiple adsorption sites where molecule can sit. In our case, the surface is composed of Co and Ir atoms, thus we need to consider following sites; top of Co atom (A-site), top of Ir atom (B-site), top of Cr atom of the

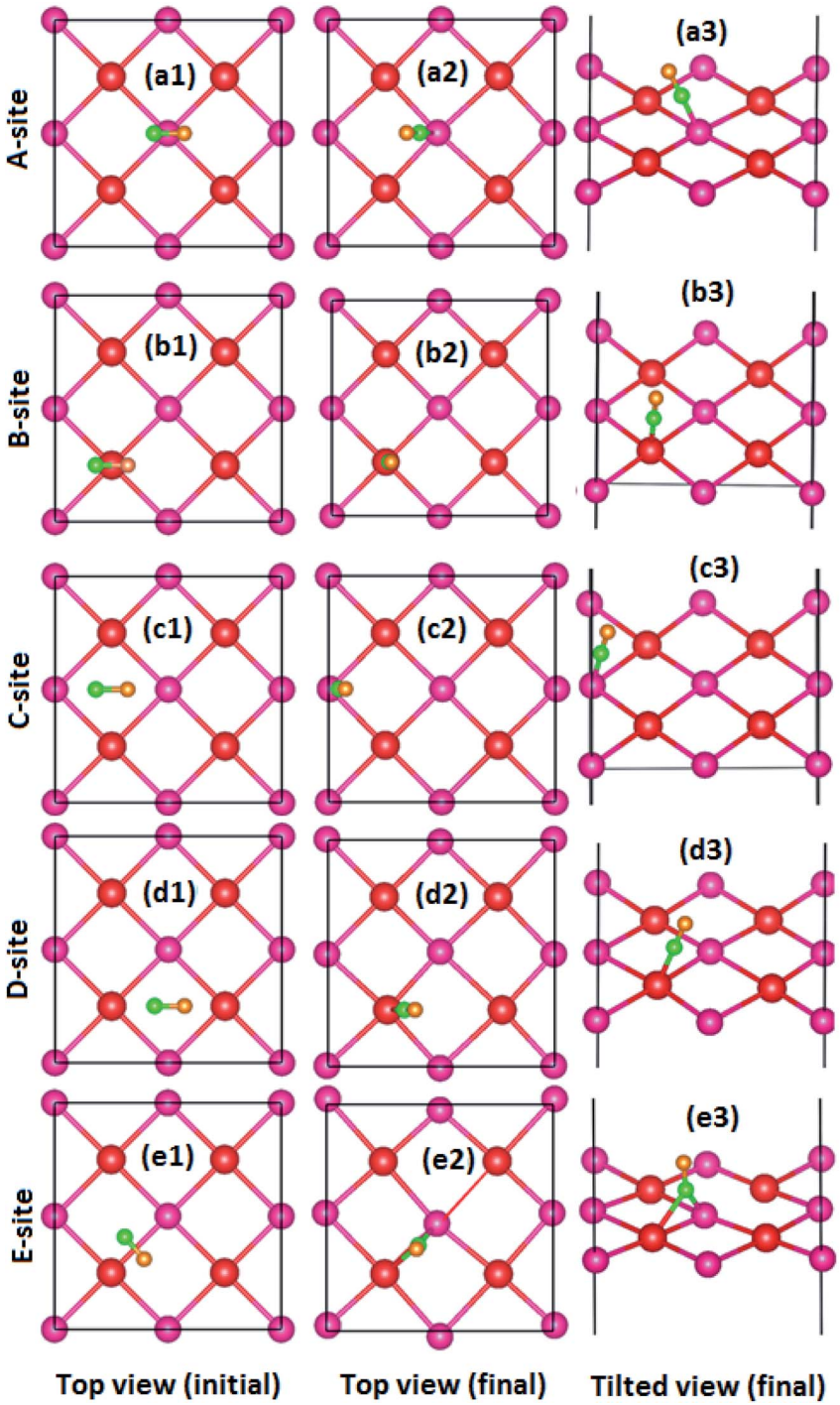

Fig. 4 (a1, a2, a3) Top (initial), top (final) and tilted (final) view for CO adsorbed at A-site, (b1, b2, b3) top (initial), top (final) and tilted (final) view for CO adsorbed at B-site, (c1, c2, c3) top (initial), top (final) and tilted (final) view for CO adsorbed at C-site, (d1, d2, d3) top (initial), top (final) and tilted (final) view for CO adsorbed at D-site, (e1, e2, e3) top (initial), top (final) and tilted (final) view for CO adsorbed at E-site.

© 2022 The Author(s). Published by the Royal Society of Chemistry

second layer (C-site), top of Ga atom of the second layer (D-site), and on the bridge of Co–Ir bond (E-site), shown in Fig. 1(b).

Isolated CO molecule. Before discussing the adsorption mechanism of CO, we first analyze the geometry and electronic properties of the isolated CO gas molecule, presented in Fig. 3(a and b). As is known, CO is a planar molecule, formed through a double bond between carbon and oxygen atom. In the fully relaxed form, C–O bond length is found to be 1.114 Å, in agreement with that reported elsewhere.[46] From the TDOS plots, we find that molecule exhibits some well symmetric and sharp electronic states around −21 eV, −6 eV, 4 eV, E_F, 7 eV and 9 eV. From the ODOS plots (Fig. 3(b)) one can find that these sharp peaks, in fact, originate from the hybridization between O-s/p and C-s/p orbitals.

CO adsorbed CrCoIrGa(001) surface. The post adsorption geometries in various configurations are displayed in Fig. 4. For A-site where CO molecule is initially placed above the surface in such a way that the distance between the center of mass of the molecule and the Co atom of the ML-1 is about 1.50 Å (see Fig. 4(a1))). After relaxation, the molecule attains an inclined configuration with C (O) atom pointing toward (away) the surface. The C–Co distance d_{C-Co} is reported to be 1.74 Å, being shorter than the sum of covalent radii of Co and C represented by R(Co and C) of 2.26 Å. The Co–O distance is 2.91 Å, being significantly greater than the R(Co and O) of 2.16 Å, confirms that Co does interacts chemically with CO through C atom. The vertical height h between A-site Co atom and C atom (of the molecule) is 1.634 Å, a justification of the vertical displacement of the molecule away from the surface. In B-site, the molecule

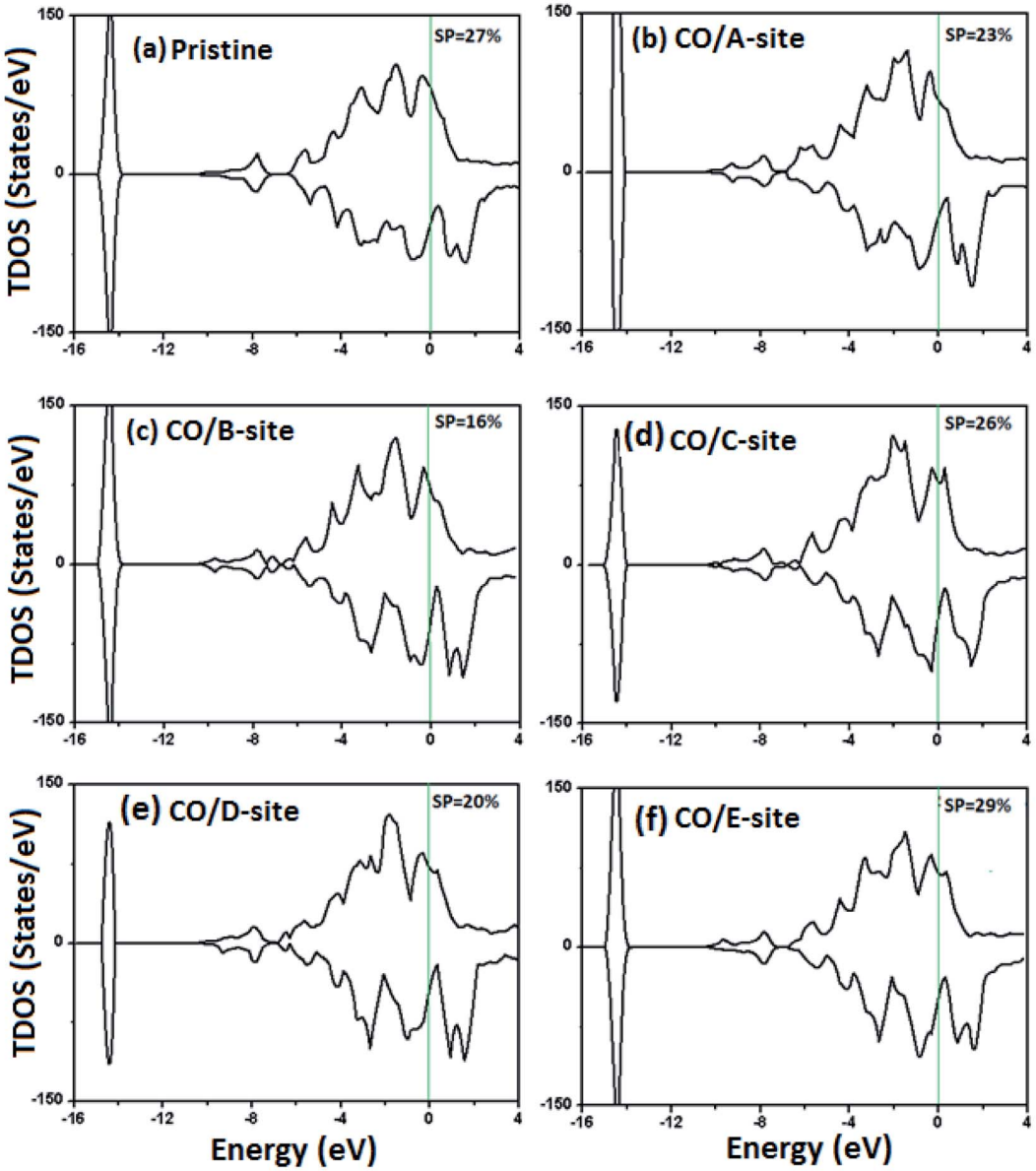

Fig. 5 Total density of states (TDOS) for (a) pristine surface, (b–f) CO adsorbed surface.

© 2022 The Author(s). Published by the Royal Society of Chemistry

occupies an initial horizontal position on the top of Ir atom. After relaxation, it rotates about 180 degrees and becomes attached vertically with Ir atom, through C–Ir bonding. The computed C–Ir distance d_{C-Ir} of 1.74 Å is shorter than the R(C and Ir) value of 2.2 Å, and the (C to Ir) h value of 1.86 Å, collectively provide an indication of some significant

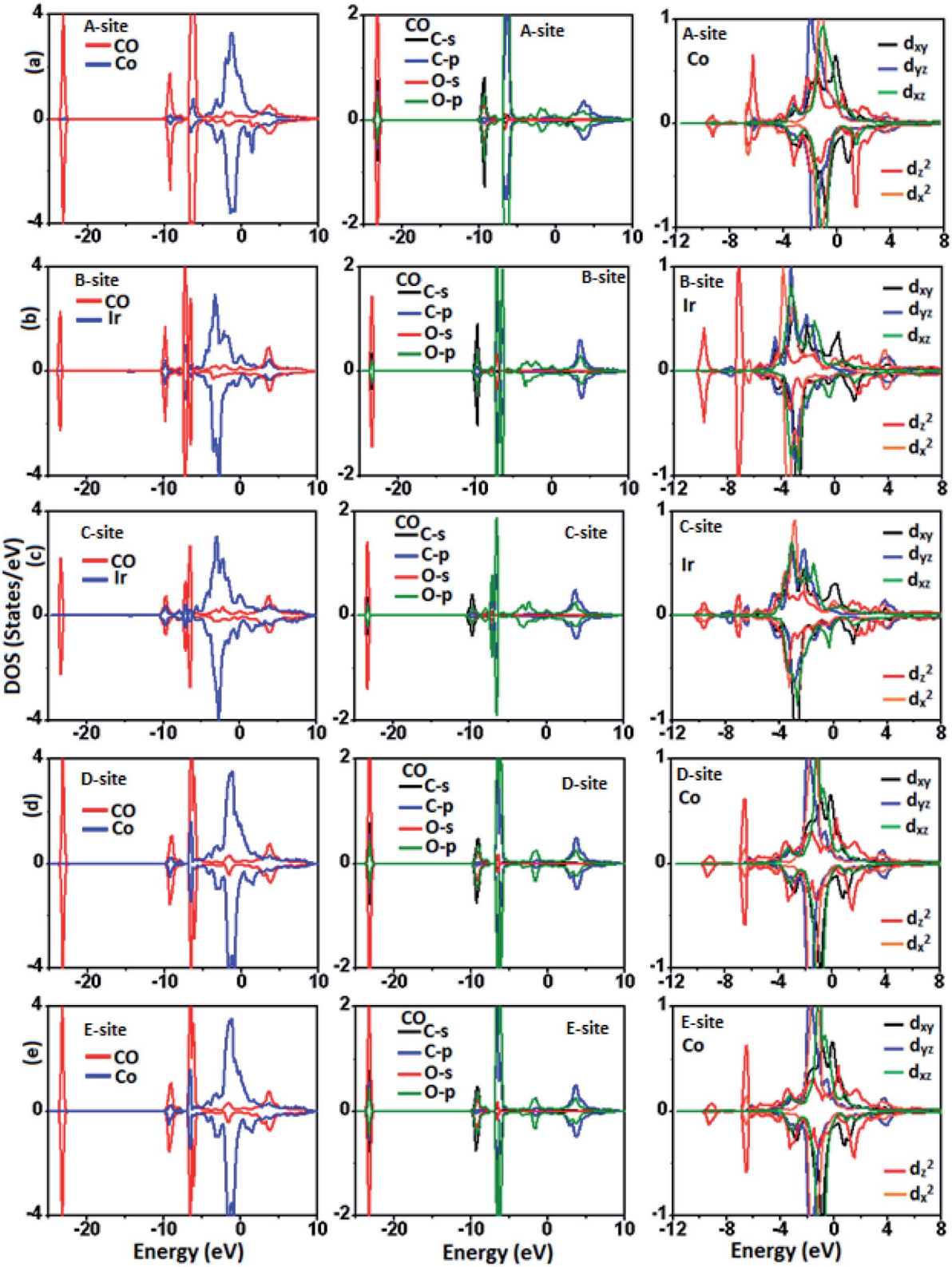

Fig. 6 Partial and orbital density of states (PDOS and ODOS) for CO molecule adsorbed CrCoIrGa(001) surface.

© 2022 The Author(s). Published by the Royal Society of Chemistry

interaction strength between molecule and Ir atom of the surface. The C- and D-sites, the hollow site among Co and Ir atoms, are found to be unstable adsorption sites, because, the molecule moves to other sites after relaxation and gets connected with Co, and Ir atoms, respectively. However, the D-site the bridge site, shows some interesting features. For example, C atoms interact with both Co and Ir atoms by forming bonds with Co and Ir atoms, with d_{C-Co} of 1.80 Å and d_{C-Ir} of 2.18 Å.

The strength and nature of the interaction between adsorbate (CO) and adsorbent (surface) can be well estimated from the adsorption energy E_a and Bader charge ΔQ, listed in Table 1. For CO/A-site, E_a is of -2.115 eV and ΔQ is -0.278e, where negative sign of E_a indicates that interaction between adsorbent and adsorbate is energetically favorable, while the negative value of ΔQ shows that charge is transferred from surface to CO molecule. In addition, the system achieves E_F of 1.454 eV and spin-polarization SP of 23%, respectively, being less than the value of E_F (1.462 eV) and SP (27%) found in CO free system. Furthermore, CO adsorption results in decrease in total magnetic moment M from 43.435 μ_B to 41.808 μ_B. These findings collectively prove that two reactants have strong interaction between them (chemisorption).

The atomic origin of interaction between CO and surface atoms can be well explored from the DOS plots of the Co/Ir atoms connected to CO molecule shown in Fig. 5 and 6. We find that, in the presence of CO molecule, the SP of the surface is slightly changed. Pristine surface (without CO) has SP value of 27%, which decreases to 23% and 16% for A-site and B-site adsorption. On the other hand, SP value shows less deviation from the actual value (only 2% increased). The observed change in SP, can be probed with atomic DOS plots. As discussed in the beginning that isolated CO molecule has symmetric distribution of majority/minority electronic states over the entire energy range, signifying the hybridization between C and O atoms. It would be useful to explore the effect of adsorption on the electronic behavior of the gas molecule. On comparing Fig. 3(a) with Fig. 6(a), it is obvious that, in vicinity of surface, the electronic states of the CO molecule redistribute around the Fermi level, as energy states are shifted to lower energy side, and there is hybridization between C-p and Co/Ir-d orbitals. These

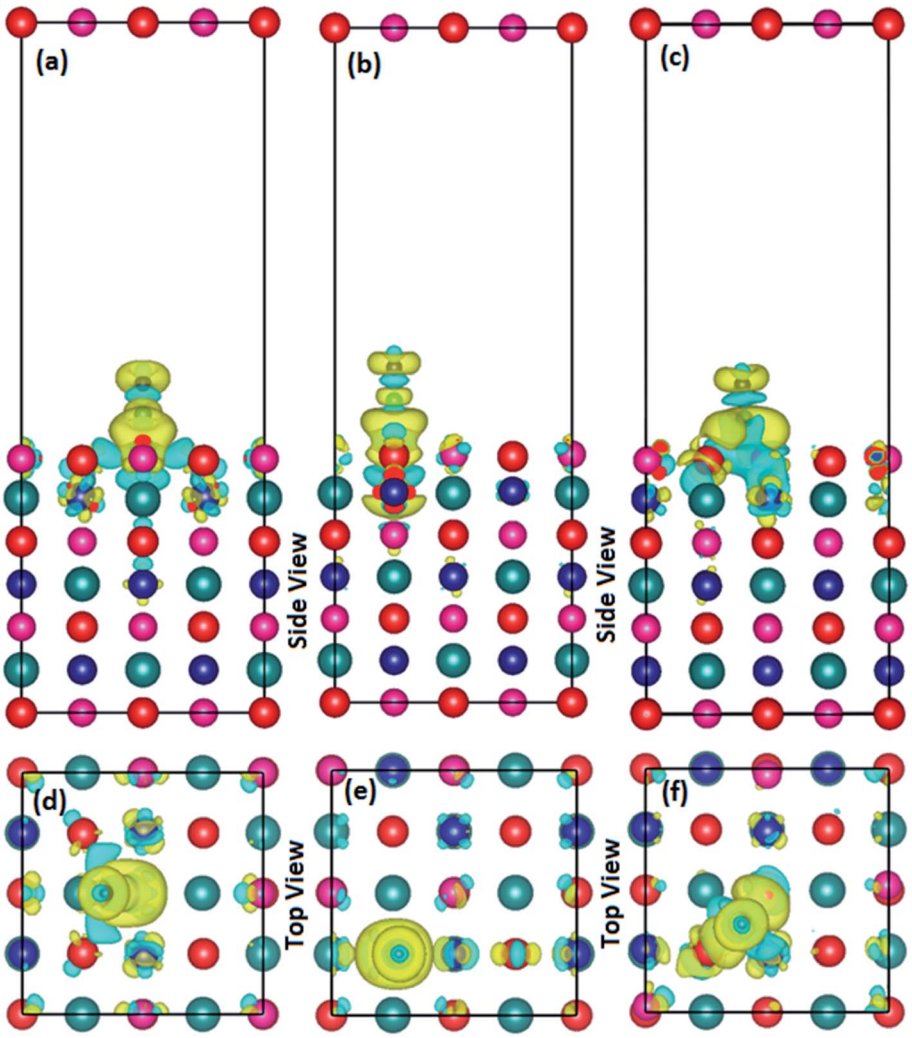

Fig. 7 Charge density difference (CDD) plots for CO adsorbed at A-site (a and d), B-site (b and e) and D-site (c and f) of the CrCoIrGa(001) surface. The yellow (cyan) color represents charge accumulation (depletion) region, and the iso-surface value is set at 1.5×10^{-3} e Å^{-3}.

© 2022 The Author(s). Published by the Royal Society of Chemistry

electronic interactions result in stabilizing the CO molecule over the surface and designating adsorption energy and charge transfer. The charge transfer ΔQ between adsorbate and adsorbent is regarded as a parameter to estimate the strength of interaction. For strong chemical interactions (chemisorption) ΔQ to known to have large value, and there would be physisorption for very small ΔQ values.[46] The ΔQ value is taken negative if charge transfer takes place from surface to molecule, as found in our case. The charge density difference (CDD) plots, gives a physical picture of electronic charge redistribution (CR) in a chemical process. The CDD plots shown in Fig. 7, show that, there is CR at the adsorption sites, such that the surface donates charge (cyan) to the molecule (yellow), as found in Bader charge analysis. The CCD plots, along with E_a, ΔQ, h, d_{min}, E_F and ΔM data, predict that the given surface has tendency to capture the CO molecule. For practical gas sensing applications, sensors with moderate adsorption energy are desired to be used in a reversible manner. Having reasonable adsorption energy, and large charge transfer from adsorbent to adsorbate, short interaction distance for all these configurations, we thus can predict that CO strongly interacts (chemisorption) with CrCoIrGa(001) thin film surface, that could be considered in gas sensing applications.

Conclusion

Herein, the adsorption properties of CO gas molecule over the CoIr-terminated CrCoIrGa(001) surface of the quaternary Heusler alloy CrCoIrGa, have been explored with DFT+U calculations. The results reveal that pristine surface reserves the bulk atomic structure, exhibiting no apparent surface reconstruction. Owing to the emergence of unsaturated bonds at the surface, the surface atoms carry enhanced magnetic moments and spin-polarization. The interaction between CO and surface is explored at five different sites with computed density of states (DOS), adsorption energy (E_a), change in magnetic moment (ΔM), vertical height between molecule and surface (h), charge transfer (ΔQ), and charge density difference (CDD) plots. For all configurations, the E_a lies in the range of -2.15 to -2.34 eV, with CO molecule adsorbed on the top of Ir atom as the most favorable configuration. The Bader charge analysis shows that CO molecule acts as a charge acceptor, by taking charge from the surface atoms. The observed E_a, ΔQ, h, and ΔM values prove that CO molecule has chemisorption over the surface, and thus the alloy surface could be used in gas sensing applications.

Conflicts of interest

The authors have no conflict of interest.

Acknowledgements

The authors extend their appreciation to the Deanship of Scientific Research at King Khalid University for the financial support through research groups program under grant number (R.G.P.2-74-43).

References

1 A. A. I. A. S. Komaladewi, P. T. P. Aryanti, I. D. G. A. Subagia and I. G. Wenten, *J. Phys.: Conf. Ser.*, 2019, **1217**, 012046.
2 S. Andersson and J. B. Pendry, *Phys. Rev. Lett.*, 1979, **43**, 363–366.
3 J. M. Gottfried, K. J. Schmidt, S. L. M. Schroeder and K. Christmann, *Surf. Sci.*, 2003, **536**, 206–224.
4 J. F. Espinal, A. Montoya, F. Mondragón and T. N. Truong, *J. Phys. Chem. B*, 2004, **108**, 1003–1008.
5 C. Rohmann, J. B. Metson and H. Idriss, *Surf. Sci.*, 2011, **605**, 1694–1703.
6 C. T. Wang and M. T. Chen, *Sens. Actuators, B*, 2010, **150**, 360–366.
7 H. Bao, Y. Qiu, X. Peng, J. A. Wang, Y. Mi, S. Zhao, X. Liu, Y. Liu, R. Cao, L. Zhuo, J. Ren, J. Sun, J. Luo and X. Sun, *Nat. Commun.*, 2021, **12**, 238.
8 H. Idriss and J. Llorca, *Catalysts*, 2019, **9**(7), 598.
9 Y. He, C. J. Weststrate, D. Luo, J. W. Niemantsverdriet, K. Wu, J. Xu, Y. Yang, Y. Li and X. Wen, *Appl. Surf. Sci.*, 2021, **569**, 151045.
10 C. J. Zhang, R. J. Baxter, P. Hu, A. Alavi and M. H. Lee, *J. Chem. Phys.*, 2001, **115**, 5272–5277.
11 T. Rathi, V. R. Kumbhare and M. K. Majumder, *2020 IEEE 7th Uttar Pradesh Section International Conference on Electrical, Electronics and Computer Engineering (UPCON)*, 2020, pp. 1–5.
12 S. Idrissi, H. Labrim, S. Ziti and L. Bahmad, *J. Supercond. Novel Magn.*, 2020, **33**, 3087–3095.
13 S. Idrissi, S. Ziti, H. Labrim, L. Bahmad, I. El Housni, R. Khalladi, S. Mtougui and N. El Mekkaoui, *J. Alloys Compd.*, 2020, **820**, 153373.
14 S. Idrissi, S. Ziti, H. Labrim, R. Khalladi, S. Mtougui, N. El Mekkaoui, I. El Housni and L. Bahmad, *Phys. A*, 2019, **527**, 121406.
15 S. Idrissi, S. Ziti, H. Labrim and L. Bahmad, *J. Low Temp. Phys.*, 2021, **202**, 343–359.
16 S. Idrissi, L. Bahmad, R. Khalladi, I. El Housni, N. El Mekkaoui, S. Mtougui, H. Labrim and S. Ziti, *Chin. J. Phys.*, 2019, **60**, 549–563.
17 S. Idrissi, S. Ziti, H. Labrim and L. Bahmad, *Multidiscip. Model. Mater. Struct.*, 2021, **17**, 552–566.
18 A. Kundu, S. Ghosh, R. Banerjee, S. Ghosh and B. Sanyal, *Sci. Rep.*, 2017, **7**, 1803.
19 S. Amara, S. Labidi, R. Masrour, A. Jabar and M. Ellouze, *Chem. Phys. Lett.*, 2022, **787**, 139261.
20 I. Ait Elkoua, R. Masrour and A. Jabar, *J. Cryst. Growth*, 2021, **576**, 126381.
21 R. Masrour and A. Jabar, *J. Cryst. Growth*, 2022, **579**, 126441.
22 Y. El Krimi, R. Masrour and A. Jabar, *J. Mol. Struct.*, 2020, **1220**, 128707.
23 Y. El Krimi, R. Masrour, A. Jabar, S. Labidi, M. Bououdina and M. Ellouze, *Results Phys.*, 2020, **18**, 103252.
24 Y. El Krimi, R. Masrour and A. Jabar, *Inorg. Chem. Commun.*, 2020, **121**, 108207.

© 2022 The Author(s). Published by the Royal Society of Chemistry

25 M. Y. Raia, R. Masrour, A. Jabar, A. Rezzouk, M. Hamedoun, A. Hourmatallah, N. Benzakour, K. Bouslykhane and J. Kharbach, *Chem. Phys. Lett.*, 2022, **790**, 139328.
26 R. Masrour, A. Jabar, S. Labidi, Y. El Krimi, M. Ellouze, M. Labidi and A. Amara, *Mater. Today Commun.*, 2021, **26**, 101772.
27 R. Masrour, A. Jabar and E. K. Hlil, *Intermetallics*, 2017, **91**, 120–123.
28 R. Masrour, A. Jabar, E. K. Hlil, M. Hamedoun, A. Benyoussef, A. Hourmatallah, A. Rezzouk, K. Bouslykhane and N. Benzakour, *J. Magn. Magn. Mater.*, 2017, **428**, 12–16.
29 Y. El Krimi, R. Masrour and A. Jabar, *Mater. Today Energy*, 2021, **20**, 100685.
30 V. K. Kushwaha, J. Rani, A. Tulapurkar and C. V. Tomy, *Appl. Phys. Lett.*, 2017, **111**, 152407.
31 Y. Li, G. D. Liu, X. T. Wang, E. K. Liu, X. K. Xi, W. H. Wang, G. H. Wu and X. F. Dai, *RSC Adv.*, 2017, **7**, 31707.
32 J. M. K. Al-Zyadi, A. A. Kadhim and K. L. Yao, *J. Electron Spectrosc. Relat. Phenom.*, 2018, **226**, 17–21.
33 Y. Yang, Z. Y. Feng and J. M. Zhang, *Mater. Chem. Phys.*, 2019, **224**, 93–99.
34 R. Paudel, J. C. Zhu, M. K. Hussain, M. Batouche, M. Waqas Qureshi and D. Paudyal, *J. Magn. Magn. Mater.*, 2021, **539**, 168425.
35 T. Kojima, S. Kameoka and A.-P. Tsai, *Sci. Technol. Adv. Mater.*, 2019, **20**, 445–455.
36 T. Kojima, S. Kameoka and A.-P. Tsai, *ACS Omega*, 2017, **2**, 147–153.
37 T. Kojima, S. Kameoka and A.-P. Tsai, *ACS Omega*, 2019, **4**, 21666–21674.
38 H. H. Hwu, J. Eng and J. G. Chen, *J. Am. Chem. Soc.*, 2002, **124**, 702–709.
39 G. Kresse and J. Furthmüller, *Phys. Rev. B: Condens. Matter Mater. Phys.*, 1996, **54**, 11169–11186.
40 J. P. Perdew, K. Burke and M. Ernzerhof, *Phys. Rev. Lett.*, 1996, **77**, 3865–3868.
41 S. Grimme, J. Antony, S. Ehrlich and H. Krieg, *J. Chem. Phys.*, 2010, **132**, 154104.
42 A. Cadi-Essadek, A. Roldan, D. Santos-Carballal, P. E. Ngoepe, M. Claeys and N. H. de Leeuw, *S. Afr. J. Chem.*, 2021, **74**, 8–16.
43 J. Y. Rhee and N. Singh, *J. Korean Phys. Soc.*, 2010, **57**, 1233–1237.
44 V. Alijani, J. Winterlik, G. H. Fecher, S. S. Naghavi and C. Felser, *Phys. Rev. B: Condens. Matter Mater. Phys.*, 2011, **83**, 184428.
45 M. Mushtaq, S. Al-Qaisi and I. U. Nabi Lone, *Solid State Commun.*, 2022, **342**, 114636.
46 M. Mushtaq, S. Godara, R. Khenata and M. Usman Hameed, *RSC Adv.*, 2021, **11**, 25217–25227.
47 K. Momma and F. Izumi, *J. Appl. Crystallogr.*, 2011, **44**, 1272–1276.

© 2022 The Author(s). Published by the Royal Society of Chemistry